Tectonics

Supporting Information for

Surface uplift and topographic rejuvenation of a tectonically inactive range: Insights from Anti-Atlas and Siroua Massif (Morocco)

Clementucci R.[1,2], Ballato P.[1], Siame L.[2], Fox M.[3], Lanari R.[1,4], Sembroni A.[1], Faccenna C.[1,5], Yaaqoub A.[6], Essaifi A.[6]

[1] Dipartimento di Scienze, Università Roma Tre, Largo San Leonardo Murialdo 1, 00146 Rome, Italy.

[2] Aix-Marseille Univ., CNRS, IRD, INRAE, Collège de France, CEREGE, Aix-en Provence, France.

[3] Department of Earth Sciences, University College London, Gower Street, London, WC1E 6BT, United Kingdom.

[4] Dipertimento di scienze, Università di Firenze, Italia.

[5] GFZ-German Research Centre for Geosciences, Potsdam, Germany.

[6] Département de Géologie, FSSM, B.P. 2390, Universite´ Cadi Ayyad, Marrakech, Morocco.

Contents of this file

Introduction

This supporting information comprises:

- A text S1 and figure S2 provide a more complete description of methods, in particular about the knickpoints analysis.
- Figure S3 and S4 with data of knickpoint and river profiles of the Anti-Atlas.
- Table S3 summarize data of the 1D river projections.

- Table S4 and figure S5 summarize the data of escavation time, estimates of erodibility parameters, used to constraint the knickpoints celerity model (results in table S5).
- Figure S6 provide the normalized channel steepness map to constraints the linear inverse model (2D projection).

S1. Knickpoints discretization and celerity model

Knickpoints can be divided in two categories, transient and stable knickpoints (Kirby and Whipple, 2012). Both features mark changes in the channel gradient, but transient knickpoints are characterized by an abrupt downstream increase in the channel steepness index reflecting a relative increase in the rate of rock uplift. Conversely, stable knickpoints are anchored in space, and are usually associated with landslides (Korup, 2006) and heterogeneities along the profile related to lithological contrasts (Kirby et al., 2003). The transient knickpoints represent a mobile boundary between the downstream portion of the landscape that has already adjusted to the new imposed rock uplift rate and the upstream part which is still recording an earlier rock uplift stage. This portion of the landscape represents the perched relict landscape that is usually bounded by migrating knickpoints (Miller et al., 2013; Olivetti et al., 2016; Gallen and Wegmann, 2017). The generation and migration of transient knickpoints can be related to changes in tectonic rates (Kirby and Whipple, 2012; Miller et al., 2013; Clementucci et al., 2022), drainage pattern reorganization associated with river capture processes (Clark et al., 2004; Willet et al., 2014; Gallen, 2018; Fox et al., 2020), base-level fall (Berlin and Anderson, 2007; Ballato et al., 2015) and/or climate changes (Crosby and Whipple, 2006; Kirby and Whipple, 2012). Distinguishing the nature of the knickpoints requires a detailed analysis of the geological and geomorphic characteristics (Kirby and Whipple, 2012). Transient and lithological knickpoints were differentiated by looking at: (1) their position and distribution in the χ-*z* plot (*i.e.*, rivers that experienced a similar rock uplift history should cluster in the χ-*z* plot; Gallen and Wegmann, 2017; Figure S2 in supporting information); (2) available geological maps (1: 200.000, 100.000 and 50.000, Service Géologique du Maroc); and (3) satellite imagery on Google Earth.

Subsequently, a celerity model was applied to calculate the onset of knickpoints migration. By using the stream model shown in equation (1), considering plucking as the primary erosion mechanism (n = 1). The horizontal migration of knickpoints along the river profiles in response to a relative base-level drop can be described as:

$$\frac{dx}{dt} = KA^m \quad (1)$$

where, dx/dt is the knickpoint celerity, K is a dimensional coefficient of erosion (Whipple and Tucker, 1999; Whipple, 2004), A is upstream drainage area and m is a non-dimensional parameter that depends on basin hydrology, channel geometry, and erosion process (Whipple and Tucker, 1999). To constrain the K and m parameters, we used a brute force two-parameter search (Stock and Montgomery, 1999; Crosby and Whipple, 2006; Berlin and Anderson, 2007; Miller et al., 2013;

Sembroni et al., 2016), which allow finding the best combination of parameters that predict the knickpoints' location. The celerity prediction has been applied over a wide range of settings and scenarios and using a large variety of constrains for *K* and *m* to minimize the misfit between the observed and modelled knickpoint positions (Berlin and Anderson, 2007; Miller et al., 2013; Ballato et al., 2015; Sembroni et al., 2016; Heidarzadeh et al., 2017). In our case, *m* was allowed to vary linearly between 0 and 0.75, as suggested by the present-day topography (Tables S1, S2 and Figure S3 in supporting information), while *K* was allowed to vary between 10^{-7} and 10^{-4} (Figure S5), in agreement with the relationship between ^{10}Be denudation rates and k_{sn}, using a linear version of the stream power model (Clementucci et al., 2022). Finally, we set the onset of knickpoints migration between 3.8 and 18.6 Ma (details in section 4.4). This timing was estimated by using the maximum excavation time required to erode the missing rock volume from the river catchments (Table S4). Although the landscape is characterized by disequilibrium condition, the estimates of denudation rate are relative only to the upper relict portion of the landscape, which is eroding at low rates (Clementucci et al., 2022). Similarly to previous studies (Norton et al. 2008; Gallen et al., 2013; Siame et al., 2015), the excavation time is expressed as:

$$T = \left(\frac{V}{A}\right) E^{-1} \qquad (2)$$

where *T* is the time required to erode the missing rock volume in the catchments, *V* is the rock volume, *A* is the drainage area of the catchments and *E* is the basin-wide denudation rate. *V* can be estimated by the difference between a surface connecting the highest points in the current landscape and the current topography itself.

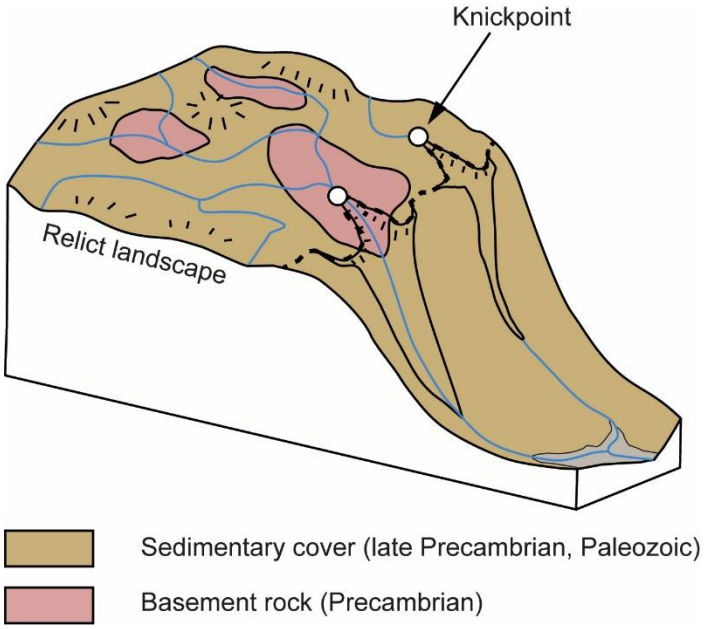

Figure S1. Cartoon of the Anti-Atlas topography. The major lithological contrast is between crystalline/ methamorphic Precambrian rock and late Precambrian/ Paleozoic sedimentary cover.

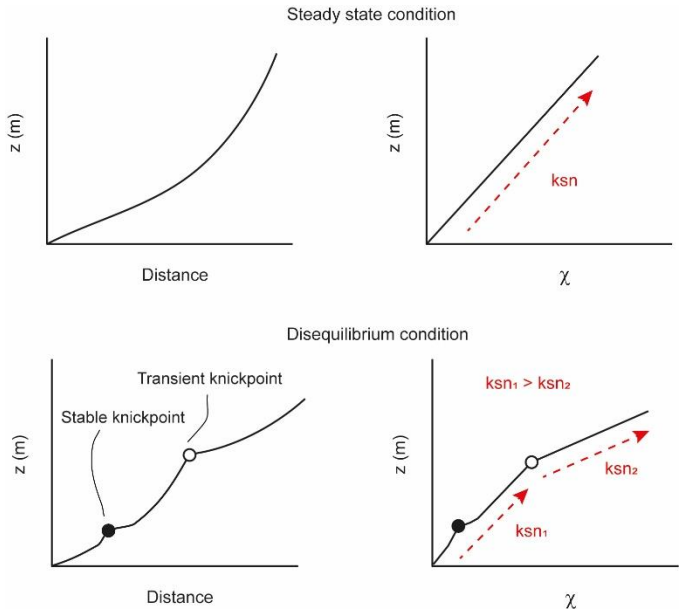

Figure S2. The simplified sketch of longitudinal river profiles (to the left) and χ-plot (to the right) in a steady-state condition and disequilibrium state. In a steady-state condition, the river can be well explain by a single value of k_{sn}, thus a straight line in a χ space (top). In a disequilibrium condition, the river is characterized by knickpoints. The transient knickpoints show an abrupt break in the χ-plot reflected the variation of rock uplift. Whereas, the stable knickpoints (lithological, dam, landslide, local heterogeneities or climate related) is not characterized by k_{sn} variation in along the profile.

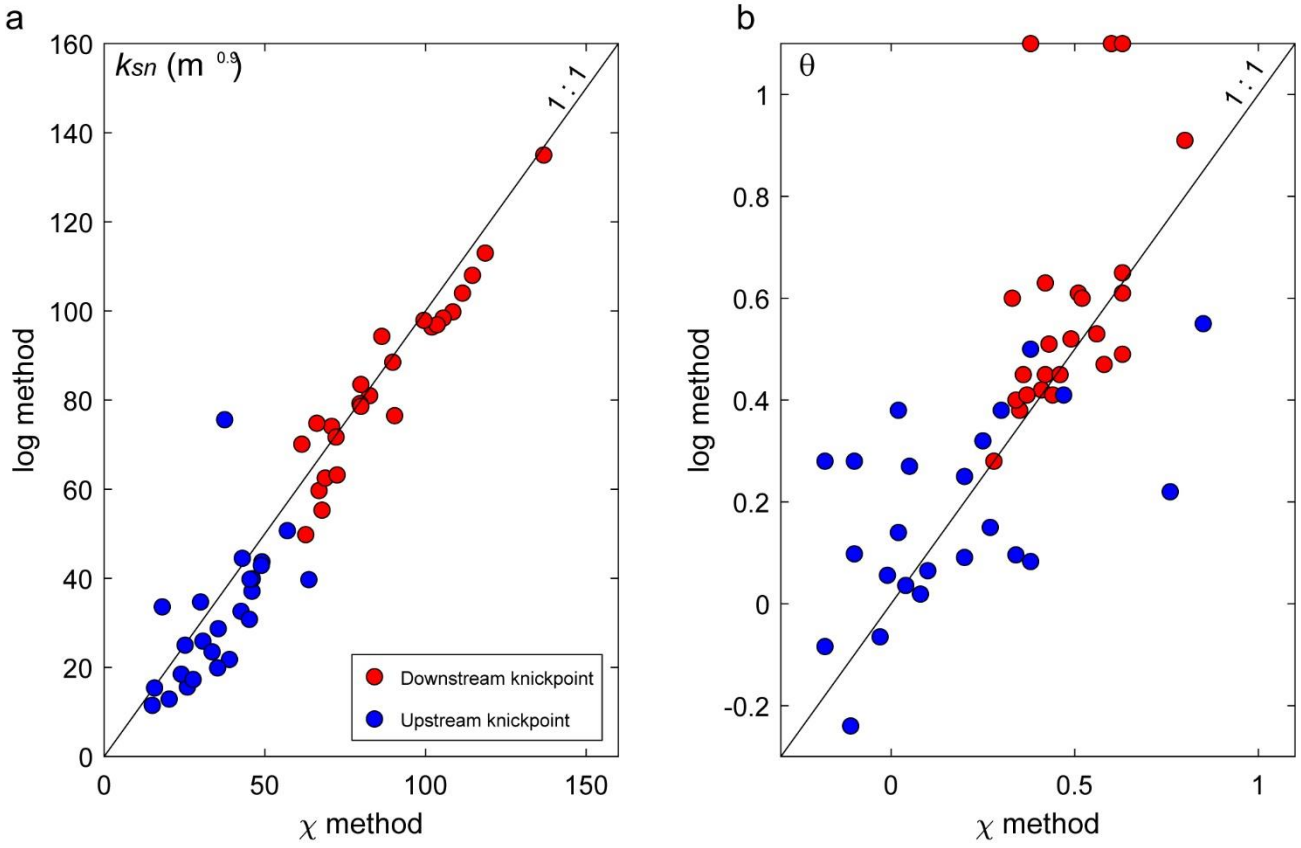

Figure S3. Comparison normalized channel steepness (k_{sn}) and concavity values (θ) using the logS-logA method and integration method (χ). Note the k_{sn} values approximately follow the 1:1 line (plot to left), whereas the concavity values are more scattered (plot to right).

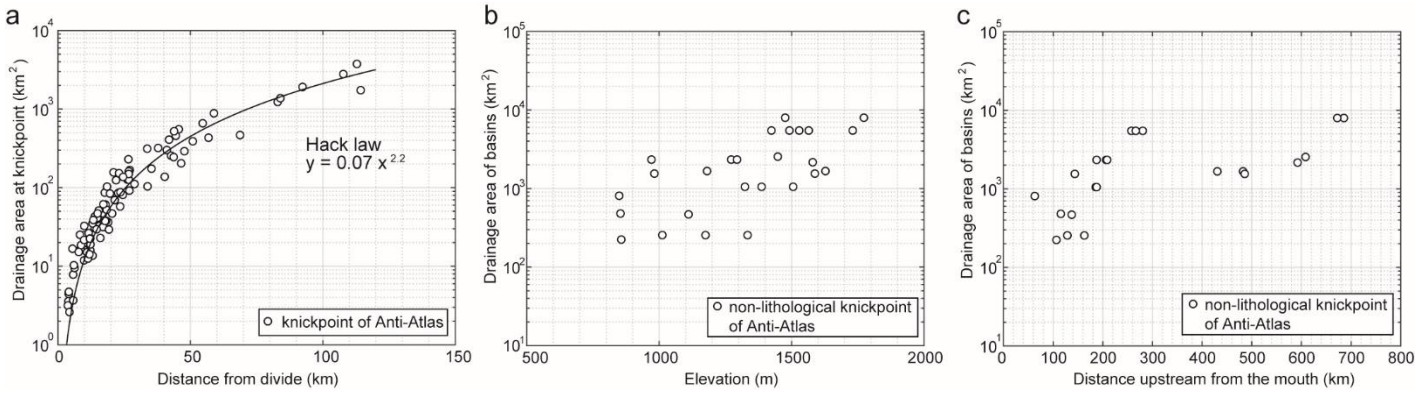

Figure S4. (a) Distance from divide versus upstream area at knickpoints location. Best-fit regression confirm the power law relation of Hack law for knickpoints in the study area. (b) Elevation of knickpoints versus drainage area of basins calculating at 500 m of elevation. (c) Distance from mouth of knickpoints versus drainage area of basins calculating at 500 m of elevation.

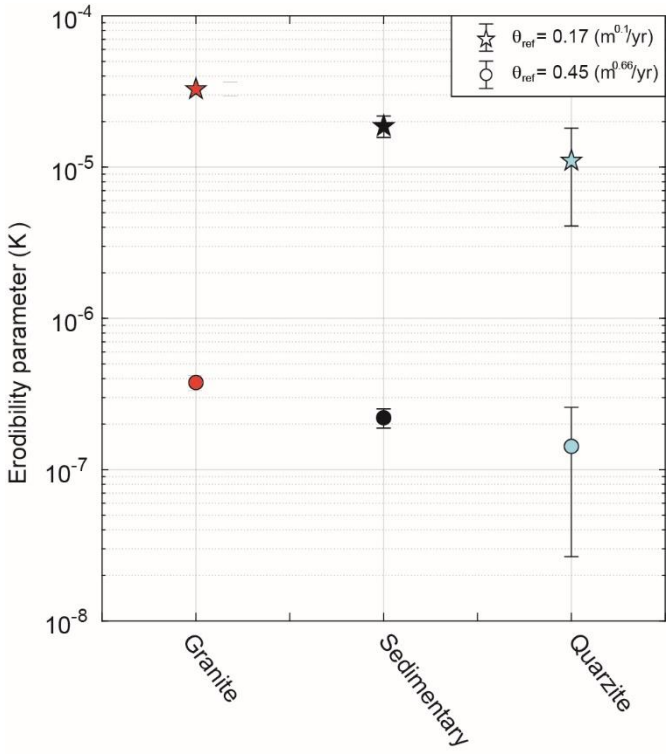

Figure S5. Rock-type versus erodibility parameter. Erodibility values were estimate from the forced linear regression between basin-wide denudation rates and basin-averaged k_{sn} using θ_{ref} of 0.45 and 0.17 (mean value of concavity relative to uplifted relict landscape, Table S1), assuming n = 1.

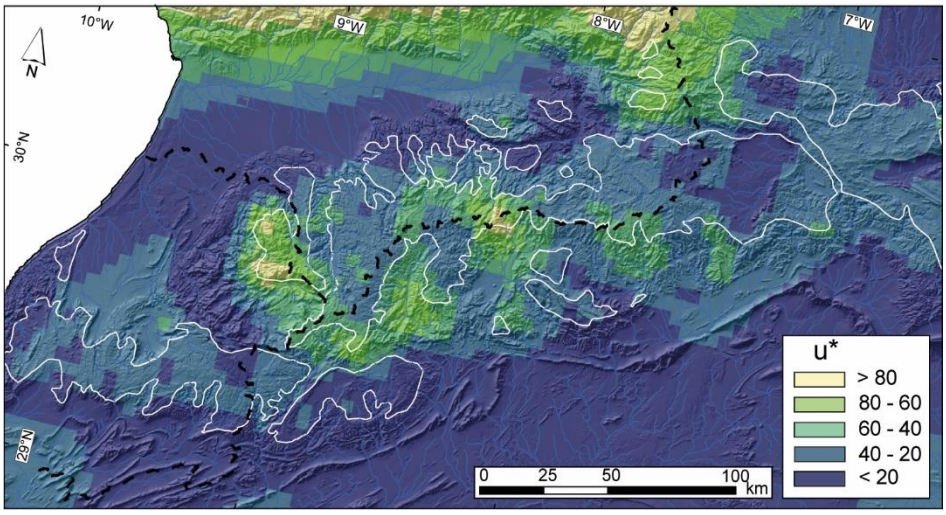

Figure S6. Normalized rock uplift rate (u^* or k_{sn}, using θ_{ref} = 0.45) map relative to the high-standing relict landscape (white polygons).

Table S3. Reconstructed relict stream profile and 95% confidence interval.

Stream[a]	m/n	Drainage divide elevation [b]	Paleo-relief [c]	Elevation knickpoint	ΔZ [d]	Error (2σ)
		(m)	(m)	(m)	(m)	(m)
NCAA1	0.45	1900	738.2	1731	1161.8	18.3
NCAA2	0.45	1900	916.1	1424	983.9	22.3
NCAA3	0.45	1900	1047.1	1565	852.9	17.4
NCAA4	0.45	1900	782.7	1492	1117.3	8.4
NCAA5	0.45	1900	903.2	1529	996.8	11.1
NCAA6	0.45	1900	1055.1	1506	844.9	42.5
NCAA7	0.45	1900	1024.1	1324	875.9	28.3
NCAA8	0.45	1900	1139.8	1387	760.2	38.4
NCAA9	0.45	1900	1054.2	1334	845.8	29.1
NCAA11	0.45	1900	1077.4	1175	822.6	36.5
Mean[e]			973.8		926.2 ± 42.1	
σ[f]					133.15	
WAA1	0.45	1400	879.5	1111	520.5	31.8
WAA3	0.45	1400	846.8	849	553.2	15.1
WAA4	0.45	1400	941.2	854	458.8	9.1
WAA5	0.45	1400	644.9	1012	755.1	15.7
WAA6	0.45	1400	760.1	982	639.9	13.9
WAA7	0.45	1400	527.9	1272	872.1	28.8
WAA9	0.45	1400	808.6	971	591.4	10.0
Mean			772.7		627.3 ± 54.1	
σ					143.17	
SCAA1	0.45	1900	1025.8	1181	874.2	5.9
SCAA2	0.45	1900	783.3	1628	1116.7	18.3
SCAA4	0.45	1900	1089.1	1588	810.9	117.7
SCAA6	0.45	1900	822.9	1448	1077.1	12.7
SCAA7	0.45	1900	824.3	1773	1075.7	58.4
SCAA8	0.45	1900	806.9	1476	1093.1	20.9
Mean			892		1008.0 ± 53.3	
σ					130.5	

[a] NCAA : rivers draining the northern flank of Anti-Atlas; WAA : rivers draining the western flank of Anti-Atlas; SCAA : rivers draining the southern flank of Anti-Atlas.

[b] Mean drainage divide elevation.

[c] Difference between mean drainage divide elevation and surface elevation (ΔZ).

[d] Estimated surface uplift from reconstructed relict stream profiles.

[e] Mean and standard error values.

[f] Standard deviation of the data.

Table S4. Maximum excavation time estimated from basin-wide denudation rates of Anti-Atlas watersheds.

Stream	Basin area[a]	Eroded material[b]	Ratio V/A [c]	Denudation rate[d] (m/Myr)		Excavation time[e] (Myr)	
	(km^2)	(km^3)	(km)	Value	Error	Value	Error
11	1200.6	148.1	0.12	7.53	0.51	16.37	0.64
10	480.1	58.6	0.12	8.10	0.55	15.07	0.59
12	842.7	117.4	0.14	12.46	0.95	11.18	0.50
9	1905.1	260.0	0.14	11.34	0.77	12.04	0.47
7	74.1	7.0	0.09	10.72	0.71	8.79	0.34
8	195.8	15.9	0.08	21.32	1.47	3.81	0.15
4	1828.1	314.7	0.17	9.25	0.65	18.61	0.76
3	558.3	56.0	0.10	5.78	0.39	17.36	0.68
5	1438.9	229.5	0.16	9.38	0.64	17.00	0.67

[a] Basin area extracted from ArcGIS.

[b] Estimated missing volume of eroded material between a smooth surface fitting the preserved summit and present-day topography (e.g., Siame et al., 2015).

[c] Ratio between volume of eroded material and basin area.

[d] Denudation rate from Clementucci et al. 2022 (^{10}Be - derived denudation rate).

[e] Ratio between eroded material from river basin and denudation rate. The values are maximum time using the denudation relative only to the relict portion of the landscape, which providing quartz grains (Clementucci et al., 2022).

References

Ballato, P., Landgraf, A., Schildgen, T. F., Stockli, D. F., Fox, M., Ghassemi, M. R., Kirby, E., & Strecker, M. R. (2015). The growth of a mountain belt forced by base-level fall: Tectonics and surface processes during the evolution of the Alborz Mountains, N Iran. *Earth and Planetary Science Letters*, 425, 204-218. https://doi.org/10.1016/j.epsl.2015.05.051

Berlin, M. M., & Anderson, R. S. (2007). Modeling of knickpoint retreat on the Roan Plateau, western Colorado. *Journal of Geophysical Research: Earth Surface*, 112(F3). https://doi.org/10.1029/2006JF000553

Clark, M. K., Schoenbohm, L. M., Royden, L. H., Whipple, K. X., Burchfiel, B. C., Zhang, X., ... & Chen, L. (2004). Surface uplift, tectonics, and erosion of eastern Tibet from large-scale drainage patterns. *Tectonics*, 23(1). https://doi.org/10.1029/2002TC001402

Clementucci, R. (2022). Deciphering mantle contribution on surface uplift in the Atlas-Meseta system (Morocco) (Doctoral dissertation). Earth Sciences. Università degli studi Roma Tre; Aix Marseille Univ. https://tel.archives-ouvertes.fr/tel-03630297/document

Crosby, B. T., & Whipple, K. X. (2006). Knickpoint initiation and distribution within fluvial networks: 236 waterfalls in the Waipaoa River, North Island, New Zealand. *Geomorphology*, 82(1-2), 16-38. https://doi.org/10.1016/j.geomorph.2005.08.023

Fox, M., & Carter, A. (2020). How continuous are the "Relict" landscapes of Southeastern Tibet?. *Frontiers in Earth Science*, 8(587597). https://doi.org/10.3389/feart.2020.587597

Gallen, S. F., Wegmann, K. W., & Bohnenstiehl, D. R. (2013). Miocene rejuvenation of topographic relief in the southern Appalachians. *GSA Today*, 23(2), 4-10. https://doi.org/10.1130/GSATG163A.1

Gallen, S. F., & Wegmann, K. W. (2017). River profile response to normal fault growth and linkage: An example from the Hellenic forearc of south-central Crete, Greece. *Earth Surface Dynamics*, 5(1), 161-186. https://doi.org/10.5194/esurf-5-161-2017

Gallen, S. F. (2018). Lithologic controls on landscape dynamics and aquatic species evolution in post-orogenic mountains. *Earth and Planetary Science Letters*, 493, 150-160. https://doi.org/10.1016/j.epsl.2018.04.029

Heidarzadeh, G., Ballato, P., Hassanzadeh, J., Ghassemi, M. R., & Strecker, M. R. (2017). Lake overspill and onset of fluvial incision in the Iranian Plateau: Insights from the Mianeh Basin. *Earth and Planetary Science Letters*, 469, 135-147. https://doi.org/10.1016/j.epsl.2017.04.019

Kirby, E., Whipple, K. X., Tang, W., & Chen, Z. (2003). Distribution of active rock uplift along the eastern margin of the Tibetan Plateau: Inferences from bedrock channel longitudinal profiles. Journal of Geophysical Research: Solid Earth, 108(B4). https://doi.org/10.1029/2001JB000861

Kirby, E., & Whipple, K. X. (2012). Expression of active tectonics in erosional landscapes. *Journal of Structural Geology*, 44, 54-75. https://doi.org/10.1016/j.jsg.2012.07.009

Korup, O. (2006). Effects of large deep-seated landslides on hillslope morphology, western Southern Alps, New Zealand. Journal of Geophysical Research: Earth Surface, 111(F1). https://doi.org/10.1029/2004JF000242

Miller, S. R., Sak, P. B., Kirby, E., & Bierman, P. R. (2013). Neogene rejuvenation of central Appalachian topography: Evidence for differential rock uplift from stream profiles and erosion rates. *Earth and Planetary Science Letters*, 369, 1-12. https://doi.org/10.1016/j.epsl.2013.04.007

Norton, K. P., von Blanckenburg, F., Schlunegger, F., Schwab, M., & Kubik, P. W. (2008). Cosmogenic nuclide-based investigation of spatial erosion and hillslope channel coupling in the transient foreland of the Swiss Alps. *Geomorphology*, 95(3-4), 474-486. https://doi.org/10.1016/j.geomorph.2007.07.013

Olivetti, V., Godard, V., Bellier, O., & ASTER team. (2016). Cenozoic rejuvenation events of Massif Central topography (France): Insights from cosmogenic denudation rates and river profiles. *Earth and Planetary Science Letters*, 444, 179-191. https://doi.org/10.1016/j.epsl.2016.03.049

Siame, L. L., Sébrier, M., Bellier, O., Bourlès, D., Costa, C., Ahumada, E. A., Gardini C. E., & Cisneros, H. (2015). Active basement uplift of Sierra Pie de Palo (Northwestern Argentina): rates and inception from10Be cosmogenic nuclide concentrations. *Tectonics,* 34(6), 1129-1153. https://doi.org/10.1002/2014TC003771

Sembroni, A., Molin, P., Pazzaglia, F. J., Faccenna, C., & Abebe, B. (2016). Evolution of continental-scale drainage in response to mantle dynamics and surface processes: An example from the Ethiopian Highlands. *Geomorphology,* 261, 12-29. https://doi.org/10.1016/j.geomorph.2016.02.022

Stock, J. D., & Montgomery, D. R. (1999). Geologic constraints on bedrock river incision using the stream power law. *Journal of Geophysical Research: Solid Earth*, 104(B3), 4983-4993. https://doi.org/10.1029/98JB02139

Whipple, K. X., & Tucker, G. E. (1999). Dynamics of the stream-power river incision model: Implications for height limits of mountain ranges, landscape response timescales, and research needs. *Journal of Geophysical Research: Solid Earth*, 104(B8), 17661-17674. https://doi.org/10.1029/1999JB900120

Willett, S. D., McCoy, S. W., Perron, J. T., Goren, L., & Chen, C. Y. (2014). Dynamic reorganization of river basins. *Science*, 343(6175). https://doi.org/10.1126/science.1248765